Interface properties of magnetic tunnel junction $La_{0.7}Sr_{0.3}MnO_3/SrTiO_3$ superlattices studied by standing-wave excited photoemission spectroscopy

A. X. Gray,[1,2] C. Papp,[2,3] B. Balke,[2,4] S.-H. Yang,[5] M. Huijben,[6] E. Rotenberg,[7] A. Bostwick,[7] S. Ueda,[8] Y. Yamashita,[8] K. Kobayashi,[8] E. M. Gullikson,[7] J. B. Kortright,[2] F. M. F. de Groot,[9] G. Rijnders,[6] D. H. A. Blank,[6] R. Ramesh,[2,10,11] and C. S. Fadley[1,2]

[1]*Department of Physics, University of California–Davis, Davis, California 95616, USA*

[2]*Materials Sciences Division, Lawrence Berkeley National Laboratory, Berkeley, California 94720, USA*

[3]*Lehrstuhl für Physikalische Chemie II, Universität Erlangen-Nürnberg, Egerlandstraße 3, 91058, Erlangen, Germany*

[4]*Institut für Anorganische und Analytische Chemie, Johannes Gutenberg-Universität, 55099 Mainz, Germany*

[5]*IBM Almaden Research Center, San Jose, California 95120, USA*

[6]*Faculty of Science and Technology, MESA+ Institute for Nanotechnology, University of Twente, Enschede, The Netherlands*

[7]*Advanced Light Source, Lawrence Berkeley National Laboratory, Berkeley, California 94720, USA*

[8]*NIMS Beamline Station at SPring-8, National Institute for Materials Science, Hyogo 679-5148, Japan*

[9]*Department of Chemistry, Utrecht University, 3584 CA Utrecht, The Netherlands*

[10]*Department of Physics, University of California, Berkeley, California 94720, USA*

[11]*Department of Materials Science and Engineering, University of California, Berkeley, California 94720, USA*

(Received 29 September 2010; revised manuscript received 27 October 2010; published 16 November 2010)

The chemical and electronic-structure profiles of magnetic tunnel junction (MTJ) $La_{0.7}Sr_{0.3}MnO_3/SrTiO_3$ (LSMO/STO) superlattices have been quantitatively determined via soft and hard x-ray standing-wave excited photoemission, x-ray absorption and x-ray reflectivity, in conjunction with x-ray optical and core-hole multiplet theoretical modeling. Epitaxial superlattice samples consisting of 48 and 120 bilayers of LSMO and STO, each nominally four unit cells thick, and still exhibiting LSMO ferromagnetism, were studied. By varying the incidence angle around the superlattice Bragg condition, the standing wave was moved vertically through the interfaces. By comparing experiment to x-ray optical calculations, the detailed chemical profile of the superlattice and its interfaces was quantitatively derived with angstrom precision. The multilayers were found to have a small ~6% change in periodicity from top to bottom. Interface compositional mixing or roughness over ~6 Å was also found, as well as a significant change in the soft x-ray optical coefficients of LSMO near the interface. The soft x-ray photoemission data exhibit a shift in the position of the Mn 3*p* peak near the interface, which is not observed for Mn 3*s*. Combined with core-hole multiplet theory incorporating Jahn-Teller distortion, these results indicate a change in the Mn bonding state near the LSMO/STO interface. Our results thus further clarify the reduced (MTJ) performance of LSMO/STO compared to ideal theoretical expectations.

DOI: 10.1103/PhysRevB.82.205116 PACS number(s): 73.20.−r, 73.21.Cd, 78.20.Bh

I. INTRODUCTION

The properties of the $La_{0.7}Sr_{0.3}MnO_3/SrTiO_3$ (LSMO/STO) interface have been subject to a number of detailed investigations since this system was discovered to be a promising candidate for a magnetic tunnel junction (MTJ).[1–3] The MTJ of course employs the phenomenon of tunneling magnetoresistance (TMR) to conduct or block electric current depending on the relative orientation of the magnetizations of two ferromagnetic electrodes (in this case LSMO), which are separated by a thin insulating barrier (STO).[4] Studies have predicted that cubic colossal magnetoresistive LSMO should have half-metallic character in its ferromagnetic phase, which should lead to a maximum TMR effect in an MTJ.[5,6] STO, on the other hand, serves as an excellent epitaxial barrier layer and/or a substrate due to a minimal lattice mismatch with LSMO and a nearly perfect atomically flat TiO_2-terminated (001) surface.[7,8] To date, however, an LSMO/STO/LSMO MTJ with performance up to the theoretical expectations has not been realized. The highest achieved values of the TMR effect are on the order of 80%,[9–11] compared to the theoretically predicted 100%;[12] furthermore, the performance degrades faster than expected as the temperature approaches the Curie temperature (T_c) of LSMO.[10,13] The most widely accepted explanation for such behavior is the occurrence of highly localized interface phenomena in the LSMO layer near the interface with STO.[14,15] The exact nature and origin of such phenomena have been investigated by a broad range of techniques[16–20] but remain much debated. Such prior studies of LSMO/STO interfaces have revealed significant layer interdiffusion,[16,17] changes in x-ray absorption fine structure for Mn L_3 and Mn L_2 peaks at the interface with STO,[16] and severe deterioration of the ferromagnetism in LSMO near the interface.[17] Furthermore, several studies have reported the presence of a nonmetallic, nonferromagnetic "dead layer" at the interface,[17,18] however, the exact thickness of such layer is still under debate.[20] In a recent study by Tebano *et al.*,[19] evidence of orbital reconstruction, leading to suppression of the double exchange mechanism at the interface was observed in ultrathin LSMO, which provides further possible causes for the diminished MTJ performance. Interfaces are also recognized to be critical in the behavior of other magnetic tunnel junction systems, as well as many other nanoscale multilayer structures.[21–23]

Since the thicknesses of the layers involved in the MTJ are on the order of few unit cells, or tens of angstroms, a highly localized and depth-selective measurement method is necessary in order to quantitatively determine the chemical, electronic, and magnetic properties of the interface region in the LSMO film. In this paper, we employ standing-wave (SW) excited photoemission, a new technique which has been used for the characterization of several types of buried layers and interfaces.[24–26] A further novel aspect in standing-wave excited photoemission studies that is exploited in this paper is the use of both soft x rays in the 0.5–1.0 keV regime and hard x rays in the multikiloelectron volt range, with all prior SW multilayer studies having been carried out with soft x rays. In particular, here we make use of results obtained in both energy regimes to determine quantitatively the variation in multilayer properties with depth.

II. EXPERIMENTAL

The standing-wave excited photoemission technique is based on spectroscopic analysis of photoelectrons excited by a strong standing wave which is set up inside a synthetic multilayer mirror (superlattice) at the incidence angle defined by the first-order Bragg condition $\lambda_\chi = 2d_{ML} \sin \theta_{inc}$, where λ_χ is the incident photon wavelength, d_{ML} is the period of the multilayer mirror, and θ_{inc} is the grazing incidence angle. The standing wave can then be moved vertically through the sample by varying either the incidence angle (a rocking curve) or the photon energy. As the antinodes of the electromagnetic field shift vertically through the sample, they highlight various parts of the sample, resulting in depth selectivity in the photoemission. The period of the standing wave is equal to the period of the superlattice, which has been in the range 20–40 Å for prior studies, and, based upon prior studies, the vertical resolution of this depth-selective photoemission technique approaches 1/10 of the standing-wave period (2–4 Å).[26] This kind of resolution should enable us to selectively probe individual monolayers of materials such as LSMO [3.88 Å unit-cell (u.c.) thickness] and STO (3.91 Å unit-cell thickness).

LSMO/STO superlattices were fabricated on TiO_2-terminated (001) single-crystal STO substrates by pulsed laser deposition, with reflection high-energy electron-diffraction (RHEED) control of the growth process, as discussed below and in the supplementary material.[37] The growth process was optimized in a previous study to result in an ideal unit-cell-controlled layer-by-layer growth and bulk-like magnetic and transport properties.[18] The RHEED intensity oscillations during growth of successive layers indicate control on the u.c. scale and a layer-by-layer growth mode. The superlattices consist of bilayers of 4 u.c LSMO (~15.5 Å) layer and a 4 u.c. STO (~15.6 Å) layer, as schematically depicted in Fig. 1(a). After growth at 750 °C, the heterostructures were slowly cooled to room temperature in ~1 bar of oxygen at a rate of 5 K/min. to optimize the oxidation level. The low surface roughness of the complete superlattice was confirmed by atomic force microscopy and x-ray diffraction (see Ref. 37).

Soft x-ray photoemission measurements were carried out at Beamline 7.0.1 of the Advanced Light Source (Lawrence Berkeley National Laboratory) at room temperature and with an overall energy resolution 300 meV. In order to maximize standing-wave effects, the excitation energy was set to 833.2 eV, which is just below the La $3d_{5/2}$ absorption edge, and corresponds to the maximum in reflectivity, as illustrated in Figs. 1(b) and 1(c). The x-ray optical properties of LSMO, with the imaginary part measured via x-ray absorption and the real part calculated via the Kramers-Kronig transformation, exhibit a sharp peak in absorption due to the La $3d_{5/2}$ resonance effect [Fig. 1(b)], which, in turn, enhances the reflectivity of the sample [Fig. 1(c)] for an energy of 833.2 eV, just below the peak in absorption. The +/− modulation in the standing-wave strength, as measured by the electric field squared is given by $\pm 100 \times 2R^{1/2}$, where R is the reflectivity of the superlattice at a given excitation energy; thus Fig. 1(c) suggests a large ±55% for our choice of photon energy. Therefore, collecting the soft x-ray measurements at this ex-

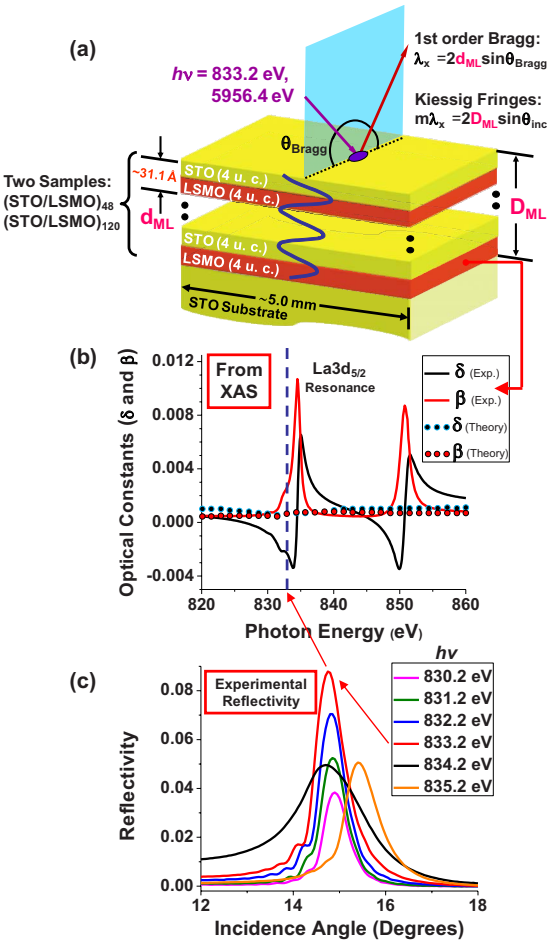

FIG. 1. (Color online) (a) Schematic of the investigated multilayer structure consisting of 48 and 120 bilayers of LSMO, grown to be 4 units cell or 15.5 Å thick, and STO, also grown to be 4 units cells or 15.6 Å thick, grown epitaxially on a single-crystal STO substrate. Photon energies of 833.2 eV corresponding to the La $3d_{5/2}$ absorption edge, and 5956.4 eV were used for the photoemission experiments. (b) X-ray optical properties of LSMO exhibit a sharp peak in absorption due to the La $3d_{5/2}$ resonance effect, which, in turn, enhances the reflectivity of the sample, as shown in (c).

citation energy near the La $3d_{5/2}$ resonance enhances the standing-wave strength, thus increasing the photoemission intensity from the regions of the sample highlighted by the standing-wave antinodes. For later reference, the tabulated optical properties of LSMO near the La $3d$ resonance,[27] which do not include near-edge resonances, are depicted with the dotted curves in Fig. 1(b) and do not exhibit the "white line" resonance peaks near 833.2 eV.

All the soft x-ray angle-resolved reflectivity measurements shown in Fig. 1(c) were carried out at Beamline 6.3.2 of the Advanced Light Source (Lawrence Berkeley National Laboratory) at room temperature and with an angular resolution of 0.01°. The beamline is equipped with a high-precision reflectometer end station, designed specifically for the purpose of characterization of multilayer mirrors. For each curve depicted in Fig. 1(c), an incidence-angle scan around the first-order Bragg angle was performed at fixed photon energy. The photon energy was then stepped in increments of 1 eV, through the La $3d_{5/2}$ resonance condition.

Hard x-ray photoemission measurements were carried out at the undulator beamline BL15XU of SPring-8 (Hyogo, Japan), also at room temperature.[28] The excitation energy was set at 5956.4 eV, a choice yielding optimum energy resolution and that is well away from any absorption edge in LSMO or STO. The overall energy resolution was 230 meV. In the case of both soft and hard x-ray photoemission, the photoemitted electrons were detected and analyzed for their kinetic energy by means of a hemispherical analyzer (VG Scienta R4000). The angle between the incident x rays and the direction of the detector was set at 60° for the soft x rays and at 90° for the hard x rays.

III. RESULTS AND DISCUSSION

In order to translate the standing wave in the direction perpendicular to the sample plane, the incidence angle was varied between 12.8° and 15.0° for the soft x rays, and between 1.79° and 1.97° for the hard x rays, thus yielding rocking curves of individual core photoelectron intensities. These experimental results were analyzed using an x-ray optical theoretical code developed by Yang *et al.*[29] which accounts for differential photoelectric cross sections and photoelectron inelastic mean-free paths in order to accurately predict the variation in photoelectron intensities with varying angle (or photon energy) and thus permits extracting depth-dependent chemical properties of the constituent layers and interfaces. The ultimate goal of the analysis was to obtain a single self-consistent model which simultaneously describes the behavior of the incidence-angle-dependent photoemission intensities from the core peaks of every element present in the structure in both the soft and hard x-ray regimes.

Figure 2 shows the final best fits between the experimental data for the 48 bilayer sample and calculated rocking curves at both energies for [(a) and (b)] Sr $3p_{3/2}$, [(c) and (d)] Ti $2p_{3/2}$, [(e) and (f)] O $1s$, (g) La $4d_{5/2}$, (h) La $3d_{5/2}$, [(i) and (j)] Mn $3p$, and [(k) and (l)] C $1s$—present as a thin surface contaminant layer. The agreement is clearly excellent, and we now briefly discuss how we arrived at these results, and what they imply for the LSMO/STO interface.

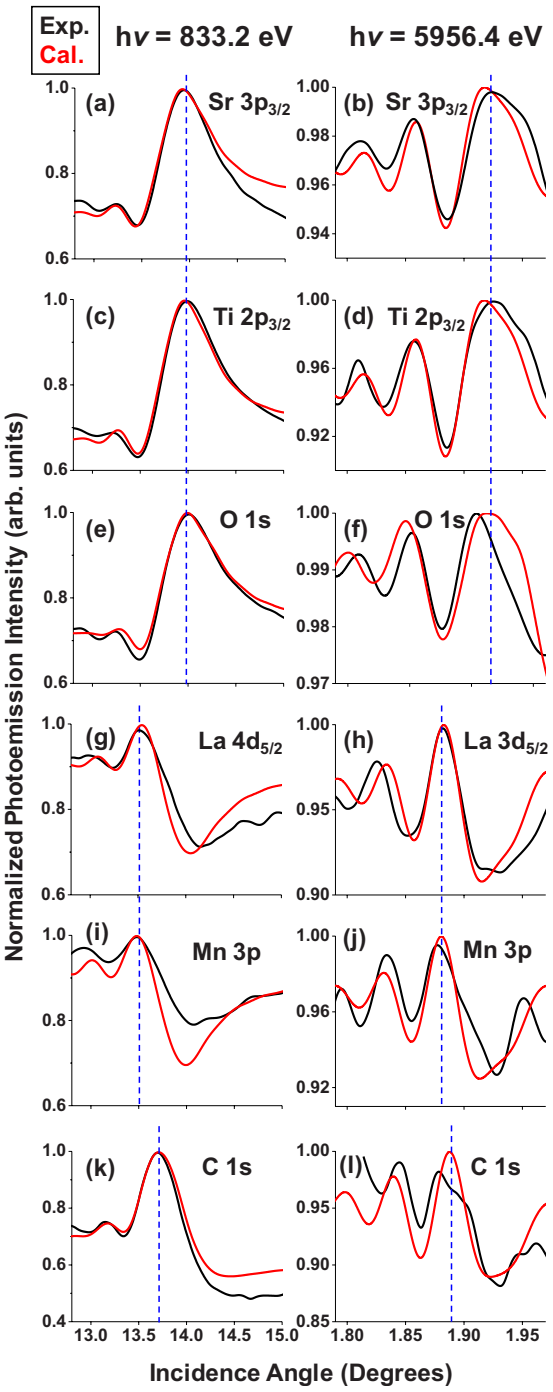

FIG. 2. (Color online) The best fits between the experimental and calculated rocking curves at 833.2 eV and 5956.4 eV for [(a) and (b)] Sr $3p_{3/2}$, [(c) and (d)] Ti $2p_{3/2}$, [(e) and (f)] O $1s$, (g) La $4d_{5/2}$, (h) La $3d_{5/2}$, [(i) and (j)] Mn $3p$, and [(k) and (l)] C $1s$. Calculations are based on a specially written x-ray optical theoretical code (Ref. 29).

All of the rocking curve spectra have two features in common—a strong peak located at an angle at which maximum photoemission from a given orbital occurs, and a series of smaller fringes on the lower-angle side of the strong peak which result from the interference between the x-ray waves reflected from the bottom of the superlattice and the top of the superlattice. The strongest feature is simply the first-

order Bragg peak of the multilayer, and the weaker peaks adjacent to it are Kiessig fringes, sometimes referred to as "Fresnel" or "interference" fringes. These fringes correspond to reflectivity maxima associated with reflection from the top and bottom of the full multilayer, with the relevant equation being $m\lambda_\chi = 2D_{ML} \sin \theta_{inc}$, where m is the order of the maximum, λ_χ is the incident photon wavelength, D_{ML} is the total thickness of the superlattice, and θ_{inc} is the grazing incidence angle. The angular frequency of the Kiessig fringes is thus determined by the total thickness of the superlattice. The Bragg and Kiessig wave components mix with relative phases to determine the relative angular positions of the peaks in intensity, and the overall structure of the rocking curve for a given orbital. Atoms at different depths in the sample will see the standing wave with a different phase and amplitude. The total intensity variation with angle finally allows us, via suitable x-ray optical analysis and simulations, to determine the thicknesses of the constituent layers in the superlattice structure.

As one immediate simple consequence of this reasoning, the Bragg peaks for all the elements comprising the STO film (Sr, Ti, and O) are located at the same angular position, and those uniquely present in the LSMO film (La and Mn) are shifted in angle. Even though Sr and O are present in both layers, the top layer (STO) dominates the shape of the rocking curves for those two elements, due to the short inelastic mean-free paths for electron escape, especially for soft x-ray excitation. We will show that the amplitude and angular position of the Kiessig fringes relative to the Bragg peak are dependent on and extremely sensitive to any kind of gradient in the thicknesses of the individual bilayers making up the superlattice. Finally, the overall amplitude, width, and shape of the rocking curves are determined by the optical properties of the constituent layers and the degree of interdiffusion between them. In general, once the effect of structural and interface fitting parameters on the shape of the rocking curve spectra is identified and understood, the exact chemical profile of the structure can be deduced in a straightforward iterative manner.

Figure 3(a) shows the final profile of the bilayer thicknesses which was necessary to assume in order to finally self-consistently describe the behavior of the rocking curves in Fig. 2 for every constituent element in the structure for both soft and hard x-ray regimes. This model incorporates a small 1 Å bottom-to-top thickness gradient for each of the LSMO and STO layers in the superlattice. That is, the thicknesses of the STO and LSMO layers at the top of the superlattice (bilayer 48) are 1 Å smaller compared to the thicknesses in the bottom bilayer (bilayer 1) which borders with the substrate, with the final optimized profile of thickness variation shown in Fig. 3(b). Extensive modeling reveals that the amplitude and the position of the Kiessig fringes relative to the Bragg peak are strongly affected by this gradient effect. To illustrate this high sensitivity, Fig. 4 demonstrates the effect of varying this thickness gradient for two simple linear thickness gradients [Fig. 4(a)] on the behavior of the rocking curves for Ti $2p_{3/2}$ [Figs. 4(b) and 4(c)] and Mn $3p$ [Figs. 4(d) and 4(e)]. For the case of a perfectly grown structure with no gradient, the Kiessig fringes (features labeled 4 and 5) should appear on both sides of the Bragg peak (features labeled 1, 2, and 3), and have relative amplitude that is ~10 times smaller than what we see in our experimental data. Also for this case, the nominal structure of the multilayer, the amplitude of the Kiessig fringes is symmetric on either side of the Bragg peak. If a gradient is present in the structure, but occurs in the opposite direction to that in Fig. 3(a) (top layers are thicker than the bottom layers), the Kiessig fringes are predicted to exhibit higher relative amplitude that is more nearly comparable with experiment, but are however, on the opposite side of the Bragg peak. This phenomenon occurs due to the shift of the angular position of the Bragg peak with respect to the Kiessig fringes. If the top layers of the superlattice are thicker than the bottom layers, the Bragg peak shifts toward a lower angular position and develops a shoulder on the lower-angle side (features labeled 6 and 7), while the Kiessig fringes remain at the same angular positions. Similarly, if the top layers of the superlattice are thinner than the bottom layers, the Bragg peak shifts toward a higher angular position and develops a shoulder on the higher-angle side, while the Kiessig fringes remain at the same angular positions. Hence, by comparing the experimen-

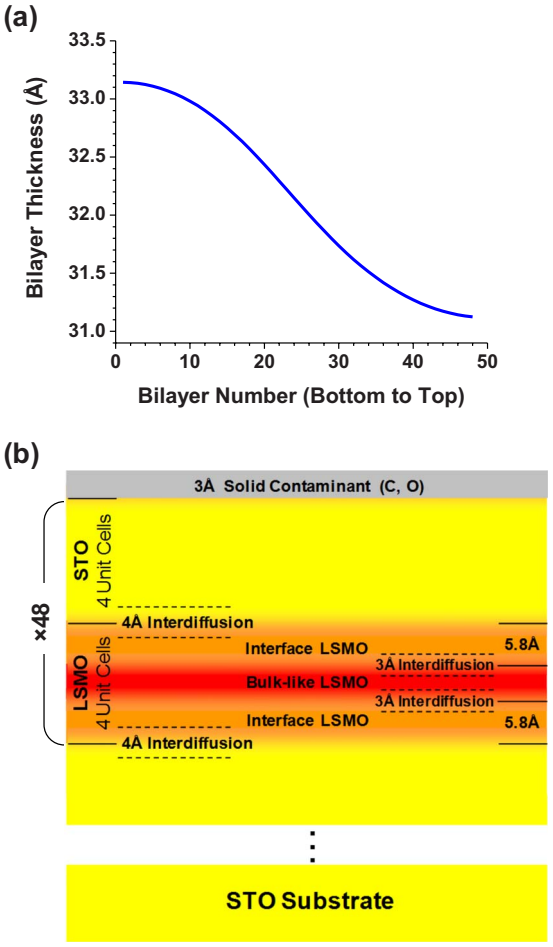

FIG. 3. (Color online) (a) The 1 Å smooth bottom-to-top thickness gradient for the thickness of the LSMO and STO layers in the superlattice that is required to fit the rocking curves in Fig. 2. (b) Model of the sample which self-consistently describes the behavior of the rocking curves for every constituent element in the structure for both soft and hard x-ray regimes.

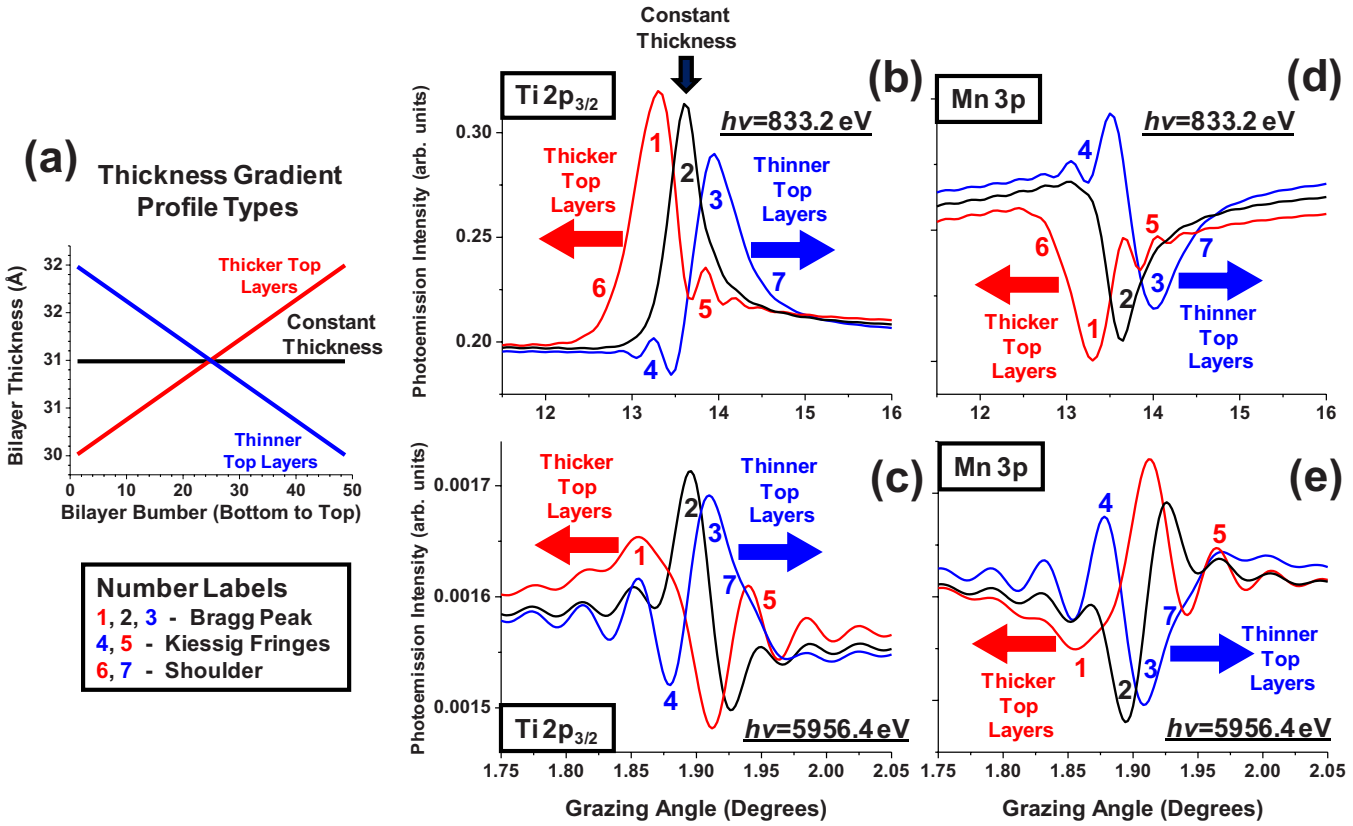

FIG. 4. (Color online) (a) Modeling the superlattice thickness gradients. Effect of simple linear thickness gradients, as well as no gradient, on the behavior of the rocking curves for [(b) and (c)] Ti $2p_{3/2}$ and [(d) and (e)] Mn $3p$ for photon energies of 833.2 and 5956.4 eV.

tal rocking curve profiles to this type of modeling, we conclude that the multilayer must contain a gradient that is in the direction shown by the curve labeled "Thinner Top Layers" in Fig. 4(a), and more quantitatively by Fig. 3(a). More broadly, such standing-wave excited photoemission spectroscopy has angstrom-level sensitivity to very small gradients in the thicknesses of the layers comprising a superlattice structure. A very small (1 Å) smooth bottom-to-top thickness gradient for the LSMO and STO layers in the superlattice could possibly be due to a slow change in the laser intensity during the 6-or-more-hour-long pulsed laser deposition growth process.

Beyond these considerations, the relative intensity of the Bragg and Kiessig features could not be fit adequately without incorporating a linear interdiffusion between the STO and LSMO layers in the superlattice. A linear interdiffusion of 4 Å was obtained by fitting the experimental data. This means that about 1 unit cell is affected by interlayer diffusion or roughness with the more surface sensitive nature of photoemission tending to measure this in the topmost unit cells of the multilayer.

Finally, a comparison of the experimental data for the La and Mn core peaks with their respective simulations revealed a gross inconsistency between the measured and calculated amplitudes of the rocking curves for these two elements that reside uniquely in the LSMO layer. The amplitudes of the experimental Bragg rocking curves were significantly suppressed, by about 1.5–2.0×, compared to the simulations (see Fig. S5 in Ref. 37). At the same time, the measured rocking curves of all other elements (Sr, Ti, O, and C) fit the model. We concluded that local electronic or dielectric inhomogeneity within the LSMO layer could be causing the suppression of the rocking curve amplitudes. Indeed, by dividing the LSMO layer into a central "bulk" component and two identical 5.8-Å-thick interfaces (top and bottom) with optical properties (refraction indices decrement δ and the absorption index β) that are different from the optical properties of bulklike LSMO, the final excellent fits between the experimental and simulated rocking curves in Fig. 2 were obtained for both Mn and La in the soft and hard x-ray regimes. We find that the La $3d_{5/2}$ resonance effects that are present in the bulklike LSMO, as depicted with solid lines in Fig. 1(b), are suppressed in the interfacial LSMO at the photon energy of 833.2 eV, resulting in the optical properties that are more consistent with the theoretical values from standard tabulations[27] at 833.2 eV, as depicted with the dashed lines. The change in the optical properties (δ and β) of LSMO at the interface with STO at the photon energy of 833.2 eV can be explained, e.g., by a change in the position, intensity, and shape of the La $3d_{5/2}$ resonance peak due to electronic interactions and changes in bonding across the interface. Such changes have been predicted using cluster calculations for a number of elements at the interfaces between two transition-metal compounds,[30] and observed experimentally using resonant inelastic x-ray scattering[31] and x-ray absorption spectroscopy,[32] and we return below to present additional

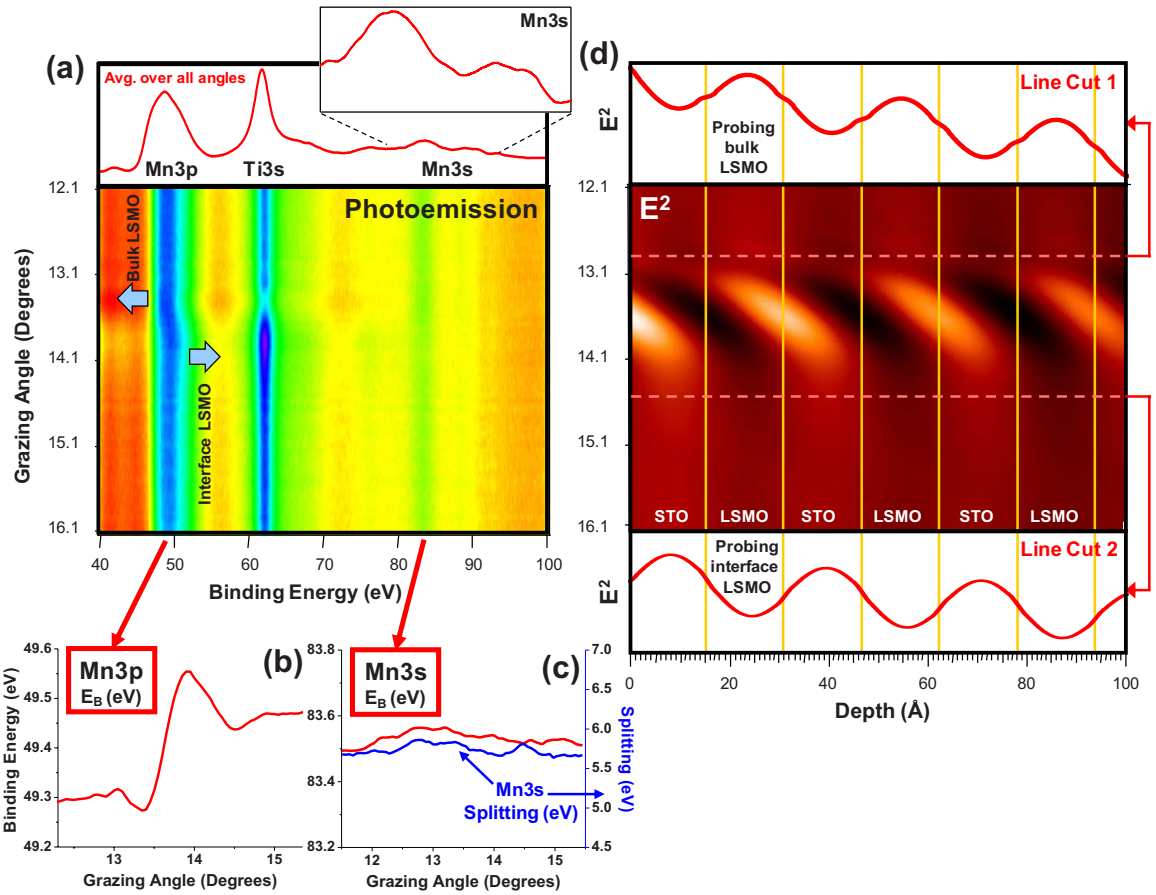

FIG. 5. (Color online) Analysis of the Mn 3*p*, Ti 2*p*, and Mn 3*s* core levels. (a) A single photoelectron spectrum over the region of Mn 3*p*, Ti 2*p*, and Mn 3*s* (which exhibits a multiplet splitting) is shown with a contour plot of the photoemission intensity as a function of incidence angle and binding energy. At the grazing incidence angle of 13.7° the Mn 3*p* core level undergoes a 0.25 eV chemical shift toward higher binding energy which persists, although getting somewhat smaller, at higher grazing incidence angles. (b) Binding energy of the Mn 3*p* peak as a function of grazing incidence angle. (c) Binding energy and multiplet splitting of the Mn 3*s* peak as a function of grazing incidence angle. (d) Intensity (E^2) of the standing-wave electric field inside the sample as a function of depth and incidence angle. The line cuts indicate that, for incidence angles $<$ 13.7°, the standing-wave field emphasizes the bulk of the LSMO layer, but for angles $>$13.7° the interface regions of the LSMO layer are highlighted. Therefore, we assign the Mn 3*p* peak shift to atoms near the interface.

evidence for this from core-level binding energy shifts seen with standing-wave excitation. The fits in Fig. 2 were refined in a final step by introducing a smooth linear interdiffusion of 3 Å between the bulk and interfacial LSMO sublayers. The results suggest that in close proximity to an epitaxial STO layer, the properties of LSMO gradually change over the distance of ~3 Å, resulting in a 5.8-Å-thick interface layer.

These results of our analysis of the rocking curves prompted a more detailed spectroscopic investigation into the properties of the LSMO layer near its interfaces with epitaxial STO. The spectra of several high-lying core levels Mn 3*p*, Ti 3*p*, and Mn 3*s* were studied with soft x-ray excitation at 833.2 eV and as a function of x-ray incidence angle. Figure 5(a) shows both a single spectrum and a contour plot of the photoemission intensity as a function of angle. The angular range from 12.1° to 16.1° covers that of the rocking curves described above. It is evident that, as the grazing incidence angle is increased through 13.7°, the Mn 3*p* core level undergoes a shift toward higher binding energy, with peak fitting yielding a maximum value of about 0.25 eV, as shown in Fig. 5(b). This shift persists, although getting somewhat smaller at about 0.17 eV, at higher incidence angles. In contrast to the Mn 3*p* core level, the contour plot shows that the Ti 3*s* core level remains at the same binding energy of 61.9 eV for the entire range of measured incidence angles, a result that is confirmed by detailed peak fitting. Another observation is that neither the Mn 3*s* binding energy, nor its exchange-related multiplet splitting shows a significant change with incidence angle, as confirmed by the peak fitting results in Fig. 5(c). A more detailed analysis of the Mn 3*p* and Mn 3*s* behavior is presented below.

To first understand the Mn 3*p* peak shift in terms of interface properties, we have modeled the intensity (E^2) of the standing-wave electric field inside the sample as a function of depth and incidence angle [Fig. 5(d)], and we observe the following. Over the rocking curve, the standing-wave antinode moves by about half a cycle, equivalent to the thickness of the LSMO layer. At incidence angles $<$13.7° (line cut 1), the antinode of the standing wave resides within the bulk of the LSMO layer, and therefore the photoemitted Mn 3*p* electrons originate more from bulk LSMO. At incidence angles

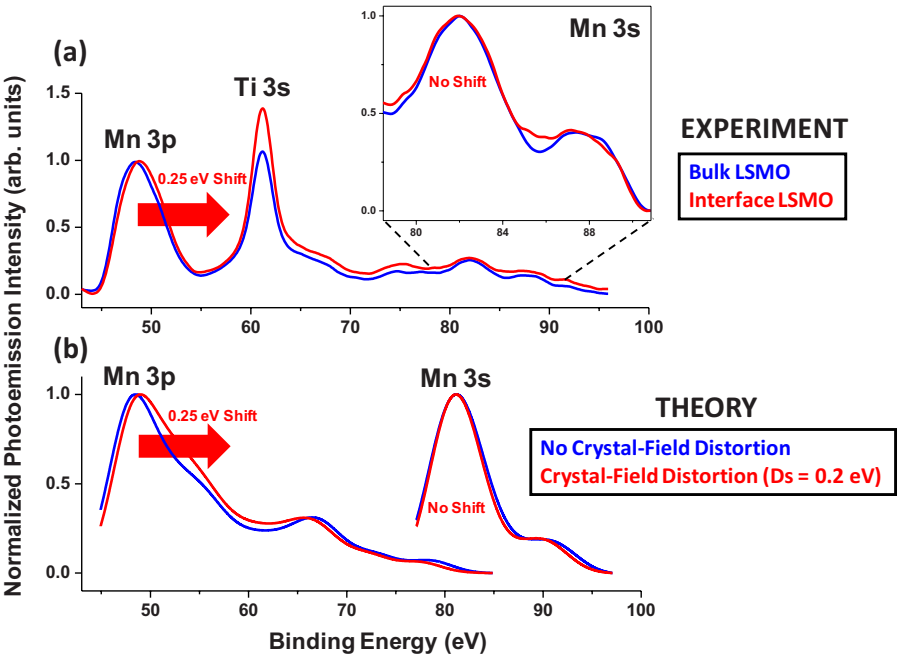

FIG. 6. (Color online) Modeling of the binding-energy shift of the Mn $3p$ and Mn $3s$ core peaks. (a) Experimental Mn $3p$ and Mn $3s$ spectra. (b) Simulated spectra using the Anderson impurity model and with and without a Jahn-Teller distortion of the lattice. The Mn $3p$ spectrum exhibits a 0.25 eV shift toward higher binding energy for the spectrum affected by Jahn-Teller, but the Mn $3s$ spectrum remains virtually unaffected, again in agreement with experiment.

$>13.7°$, (line cut 2), the interface regions of the LSMO layer are highlighted by the standing wave, and therefore the photoemitted Mn $3p$ electrons originate mainly from the interface. This interface sensitivity we expect to be a maximum for an incidence angle of 13.9°, at the maximum in Fig. 5(b). Thus we conclude that the Mn $3p$ core peak undergoes a chemical shift of ~ 0.25 eV toward higher binding energy at the interface with STO. The same interface chemical shift was observed in a thicker sample consisting of 120 LSMO/STO bilayers.

As one possible theoretical interpretation of the Mn $3p$ shift, and the lack of any change in the Mn $3s$ multiplet, we have simulated both spectra with allowance for final-state multiplet, screening, and Jahn-Teller distortions of the MnO_6 octahedra, using a well-known Anderson impurity model.[33,34] The charge-transfer multiplet program CTM4XAS (Refs. 33 and 34) was used to simulate the effects of crystal-field distortion on the spectral shapes and positions of Mn $3p$ and Mn $3s$ photoelectron spectra (see Ref. 37 for details). Our results are consistent with the presence of D_{4h} crystal-field distortion effects at the interface, which affect Mn $3p$ more than Mn $3s$ and cause a shift of the former toward higher binding energy. The best fit for the experimental data depicted in Fig. 6 was achieved by introducing a tetragonal crystal-field distortion parameter $Ds=0.2$ eV and a ligand-field splitting parameter $10Dq=1.5$ eV. Figure 6(a) compares experimental spectra with maximum bulk sensitivity with those of maximum interface sensitivity, as judged from the results of Fig. 5. Figure 6(b) compares the calculated photoelectron spectra with and without crystal-field splitting for the Mn $3p$ and Mn $3s$ core levels. The Mn $3p$ spectrum exhibits a 0.25 eV shift in peak position toward the higher binding energy for the spectrum affected by crystal-field distortion, whereas the Mn $3s$ peak position does not show such a shift. These results are thus in excellent agreement with the experimental data. The Mn $3s$ multiplet splitting calculation also predicts other features in the experimental spectra—the peaks at 82 and 88 eV, although theory predicts a somewhat larger splitting of 8.3 eV than the observed splitting of 5.7 eV; such differences have been observed before however.[33,34] This splitting is also not found to change as a function of incidence angle (i.e., standing-wave position or depth). Comparing the magnitude of the Mn $3s$ splitting with prior experimental results for a variety of Mn compounds,[35,36] we also conclude that Mn is mainly in a trivalent $3d$ (Ref. 4) configuration both at the interface and in the bulk of LSMO.

It is now worth comparing our conclusions to those of prior investigations. Recent transmission electron microscopy with electron-energy-loss spectroscopy (EELS) studies of LSMO/STO/LSMO magnetic tunneling junctions and LSMO/STO superlattices[16] revealed that the LSMO layer can be inhomogeneous at the interfaces with STO. It has been concluded that this inhomogeneity is most likely caused by interdiffusion with the STO layers and structural deformation at the interfaces, mostly induced by strain and oxygen vacancies. Our findings of the interdiffusion of STO and LSMO at the interfaces and presence of crystal-field distortion agree well with these observations. This prior study is also consistent with our results in revealing via elemental analysis that the central bulk region of the LSMO layer conforms to the established nominal composition formula, and that the "top" and "bottom" interfacial LSMO layers are symmetric about the bulklike region. Previous EELS analysis demonstrated a thickness of the interfacial LSMO layer on the order of 11–18 Å. However, our study revealed that the thickness of the interfacial LSMO layer is, in fact, smaller—specifically, 5.8 Å (+1.5 Å due to interdiffusion with the central bulklike LSMO layer). Note that our LSMO/STO superlattices, consisting of 4 u.c. LSMO and 4 u.c. STO, have thinner LSMO layers than those used in the previous study[20] but they still exhibit clear ferromagnetic behavior up to room temperature (see Ref. 37). This shows that we have reduced the critical thickness for ferromagnetism of LSMO to only 4 unit cells.

IV. CONCLUSIONS

In conclusion, by using standing-wave excited photoemission in the soft and hard x-ray regimes, in conjunction with x-ray optical theoretical calculations, we have determined the chemical and electronic structure profile of the LSMO/STO superlattice with angstrom precision. An interdiffusion region of 4–5 Å in thickness between the STO and LSMO layers was observed. Analysis of the Bragg and Kiessig features in the rocking-curve spectra also revealed a 1 Å smooth bottom-to-top thickness gradient for the LSMO and STO layers in the superlattice. Fitting of the La and Mn rocking-curve spectra further revealed that the properties of LSMO change in the proximity of the STO interface. Specifically, a 5.8-Å-thick interfacial LSMO layer characterized by optical properties (δ and β) that are different from the optical properties of the bulklike LSMO, is present at the top and bottom interfaces with STO. In particular, the La $3d_{5/2}$ resonance effects that are present in the bulklike LSMO are suppressed and/or shifted in the interfacial LSMO at the photon energy of 833.2 eV. The interfacial LSMO layers are smoothly interdiffused with the bulk LSMO layer. A more in-depth investigation into the properties of the LSMO layer revealed a 0.25 eV chemical shift of the Mn $3p$ core peak toward the higher binding energy at the interface with STO, with this shift being consistent with crystal-field distortion effects. In summary, we have provided additional evidence as to why the LSMO/STO tunnel junction does not reach the 100% TMR value expected with ideal interfaces. We have also shown that standing-wave excited photoemission can be used to study depth-dependent chemical and electronic properties of magnetic superlattice nanostructures so as to derive unique information on chemical and refractive index profiles, as well as crystal-field and magnetic moments near interfaces. Beyond this, the standing-wave excited photoemission method that we have applied to this particular system should be of broad use in the future for studying the buried layers and interfaces in many types of multilayer spintronic structures, and it should also be applicable to layered systems exhibiting ferroelectric, multiferroic, and superconducting properties, as well as to those related to semiconductor and energy-conversion devices.

ACKNOWLEDGMENTS

The authors acknowledge support from the Director, Office of Science, Office of Basic Energy Sciences, Materials Sciences and Engineering Division, of the U.S. Department of Energy under Contract No. DE-AC02-05CH11231. The authors are also grateful to HiSOR, Hiroshima University and JAEA/SPring-8 for the development of hard x-ray photoelectron spectroscopy at BL15XU of SPring-8. The experiments at BL15XU were performed under the approval of NIMS Beamline Station (Proposal No. 2009A4906). This work was partially supported by the Nanotechnology Network Project, the Ministry of Education, Culture, Sports, Science and Technology (MEXT), Japan.

[1] J. M. De Teresa, A. Barthélémy, A. Fert, J. P. Contour, R. Lyonnet, F. Montaigne, P. Seneor, and A. Vaurès, Phys. Rev. Lett. **82**, 4288 (1999).
[2] S. A. Wolf, D. D. Awschalom, R. A. Buhrman, J. M. Daughton, S. von Molnár, M. L. Roukes, A. Y. Chtchelkanova, and D. M. Treger, Science **294**, 1488 (2001).
[3] E. Y. Tsymbal, O. N. Mryasov, and P. R. LeClair, J. Phys.: Condens. Matter **15**, R109 (2003).
[4] M. Viret, J. Nassar, M. Drouet, J. P. Contour, C. Fermon, and A. Fert, J. Magn. Magn. Mater. **198-199**, 1 (1999).
[5] C. Ma, Z. Yang, and S. Picozzi, J. Phys.: Condens. Matter **18**, 7717 (2006).
[6] A. Chikamatsu, H. Wadati, H. Kumigashira, M. Oshima, A. Fujimori, N. Hamada, T. Ohnishi, M. Lippmaa, K. Ono, M. Kawasaki, and H. Koinuma, Phys. Rev. B **73**, 195105 (2006).
[7] M. Kawasaki, A. Ohtomo, T. Arakane, K. Takahashi, M. Yoshimoto, and H. Koinuma, Appl. Surf. Sci. **107**, 102 (1996).
[8] G. Koster, B. L. Kropman, G. J. H. M. Rijnders, D. H. A. Blank, and H. Rogalla, Appl. Phys. Lett. **73**, 2920 (1998).
[9] Y. Lu, X. W. Li, G. Q. Gong, G. Xiao, A. Gupta, P. Lecoeur, J. Z. Sun, Y. Y. Wang, and V. P. Dravid, Phys. Rev. B **54**, R8357 (1996).
[10] J. Sun, W. Gallagher, P. Duncombe, L. Krusin-Elbaum, R. A. Altman, A. Gupta, Y. Lu, G. Q. Gong, and G. Xiao, Appl. Phys. Lett. **69**, 3266 (1996).
[11] M. Viret, M. Drouet, J. Nassar, J. P. Contour, C. Fermon, and A. Fert, Europhys. Lett. **39**, 545 (1997).
[12] J. H. Park, E. Vescoso, H. J. Kim, C. Kwon, R. Ramesh, and T. Venkatesan, Nature (London) **392**, 794 (1998).
[13] M. Bowen, M. Bibes, A. Barthélémy, J.-P. Contour, A. Anane, Y. Lemaître, and A. Fert, Appl. Phys. Lett. **82**, 233 (2003).
[14] Y. Ogimoto, M. Izumi, A. Sawa, T. Manako, H. Sato, H. Akoh, M. Kawasaki, and Y. Tokura, Jpn. J. Appl. Phys., Part 2 **42**, L369 (2003).
[15] M. Izumi, Y. Ogimoto, Y. Okimoto, T. Manako, P. Ahmet, K. Nakajima, T. Chikyow, M. Kawasaki, and Y. Tokura, Phys. Rev. B **64**, 064429 (2001).
[16] L. Samet, D. Imhoff, J.-L. Maurice, J.-P. Contour, A. Gloter, T. Manoubi, A. Fert, and C. Colliex, Eur. Phys. J. B **34**, 179 (2003).
[17] H. Yamada, Y. Ogawa, Y. Ishii, H. Sato, M. Kawasaki, H. Akoh, and Y. Tokura, Science **305**, 646 (2004).
[18] M. Huijben, L. W. Martin, Y.-H. Chu, M. B. Holcomb, P. Yu, G. Rijnders, D. H. A. Blank, and R. Ramesh, Phys. Rev. B **78**, 094413 (2008).
[19] A. Tebano, C. Aruta, S. Sanna, P. G. Medaglia, G. Balestrino, A. A. Sidorenko, R. De Renzi, G. Ghiringhelli, L. Braicovich, V. Bisogni, and N. B. Brookes, Phys. Rev. Lett. **100**, 137401 (2008).
[20] L. Fitting Kourkoutis, J. H. Song, H. Y. Hwang, and D. A. Muller, Proc. Natl. Acad. Sci. U.S.A. **107**, 11682 (2010).
[21] M. Basletic, J.-L. Maurice, C. Carrétéro, G. Herranz, O. Copie, M. Bibes, É. Jacquet, K. Bouzehouane, S. Fusil, and A. Bar-

thélémy, Nature Mater. **7**, 621 (2008).
[22] S. J. May, P. J. Ryan, J. L. Robertson, J.-W. Kim, T. S. Santos, E. Karapetrova, J. L. Zarestky, X. Zhai, S. G. E. te Velthuis, J. N. Eckstein, S. D. Bader, and A. Bhattacharya, Nature Mater. **8**, 892 (2009).
[23] J. Hoppler, J. Stahn, Ch. Niedermayer, V. K. Malik, H. Bouyanfif, A. J. Drew, M. Rössle, A. Buzdin, G. Cristiani, H.-U. Habermeier, B. Keimer, and C. Bernhard, Nature Mater. **8**, 315 (2009).
[24] S.-H. Yang, B. S. Mun, N. Mannella, A. Nambu, B. C. Sell, S. B. Ritchey, F. Salmassi, S. S. P. Parkin, and C. S. Fadley, J. Phys.: Condens. Matter **18**, L259 (2006).
[25] B. C. Sell, S.-H. Yang, M. Watanabe, B. S. Mun, L. Plucinski, N. Mannella, S. B. Ritchey, A. Nambu, J. Guo, M. W. West, F. Salmassi, J. B. Kortright, S. S. P. Parkin, and C. S. Fadley, J. Appl. Phys. **103**, 083515 (2008).
[26] F. Kronast, R. Ovsyannikov, A. Kaiser, C. Wiemann, S.-H. Yang, D. E. Bürgler, R. Schreiber, F. Salmassi, P. Fischer, H. A. Dűrr, C. M. Schneider, W. Eberhardt, and C. S. Fadley, Appl. Phys. Lett. **93**, 243116 (2008).
[27] B. L. Henke, E. M. Gullikson, and J. C. Davis, At. Data Nucl. Data Tables **54**, 181 (1993).
[28] K. Kobayashi, M. Yabashi, Y. Takata, T. Tokushima, S. Shin, K. Tamasaku, D. Miwa, T. Ishikawa, H. Nohira, T. Hattori, Y. Sugita, O. Nakatsuka, A. Sakai, and S. Zaima, Appl. Phys. Lett. **83**, 1005 (2003).
[29] S.-H. Yang, A. X. Gray, B. S. Mun, and C. S. Fadley, program for calculating soft x-ray optical effects with strong reflectivity in x-ray photoemission and x-ray emission (unpublished).
[30] M. van Veenendaal, Phys. Rev. B **78**, 165415 (2008).
[31] L. Journel, J.-M. Mariot, J.-P. Rueff, C. F. Hague, G. Krill, M. Nakazawa, A. Kotani, A. Rogalev, F. Wilhelm, J.-P. Kappler, and G. Schmerber, Phys. Rev. B **66**, 045106 (2002).
[32] J. Chakhalian, J. W. Freeland, H.-U. Habermeier, G. Cristiani, G. Khaliullin, M. van Veenendaal, and B. Keimer, Science **318**, 1114 (2007).
[33] F. M. F. de Groot and A. Kotani, *Core Level Spectroscopy of Solids* (Taylor & Francis, London, 2008).
[34] E. Stavitski and F. M. F. de Groot, CTM4XAS, charge-transfer multiplet program, 2010.
[35] V. R. Galakhov, M. Demeter, S. Bartkowski, M. Neumann, N. A. Ovechkina, E. Z. Kurmaev, N. I. Lobachevskaya, Y. M. Mukowskii, J. Mitchell, and D. L. Ederer, Phys. Rev. B **65**, 113102 (2002).
[36] N. Mannella, A. Rosenhahn, C. H. Booth, S. Marchesini, B. S. Mun, S.-H. Yang, K. Ibrahim, Y. Tomioka, and C. S. Fadley, Phys. Rev. Lett. **92**, 166401 (2004).
[37] See supplementary material at http://link.aps.org/supplemental/10.1103/PhysRevB.82.205116 for details on superlattice growth, surface topography, crystal structure, ferromagnetism and core-hole multiplet calculations.